Monthly Notices
of the
ROYAL ASTRONOMICAL SOCIETY

MNRAS **467,** 661–673 (2017)
Advance Access publication 2017 January 15

doi:10.1093/mnras/stx112

The special growth history of central galaxies in groups and clusters

Carlo Nipoti★

Department of Physics and Astronomy, Bologna University, viale Berti-Pichat 6/2, I-40127 Bologna, Italy

Accepted 2017 January 12. Received 2017 January 6; in original form 2016 November 3

ABSTRACT

Central galaxies (CGs) in galaxy groups and clusters are believed to form and assemble a good portion of their stellar mass at early times, but they also accrete significant mass at late times via galactic cannibalism, that is merging with companion group or cluster galaxies that experience dynamical friction against the common host dark-matter halo. The effect of these mergers on the structure and kinematics of the CG depends not only on the properties of the accreted satellites, but also on the orbital parameters of the encounters. Here we present the results of numerical simulations aimed at estimating the distribution of merging orbital parameters of satellites cannibalized by the CGs in groups and clusters. As a consequence of dynamical friction, the satellites' orbits evolve losing energy and angular momentum, with no clear trend towards orbit circularization. The distributions of the orbital parameters of the central-satellite encounters are markedly different from the distributions found for halo–halo mergers in cosmological simulations. The orbits of satellites accreted by the CGs are on average less bound and less eccentric than those of cosmological halo–halo encounters. We provide fits to the distributions of the central-satellite merging orbital parameters that can be used to study the merger-driven evolution of the scaling relations of CGs.

Key words: galaxies: clusters: general – galaxies: elliptical and lenticular, cD – galaxies: evolution – galaxies: formation – dark matter.

1 INTRODUCTION

Central galaxies (CGs) in galaxy groups and clusters are typically massive early-type galaxies (ETGs) with relatively old stellar populations and little ongoing star formation. In the currently favoured formation model (Merritt 1985; Tremaine 1990; Dubinski 1998; Ruszkowski & Springel 2009), CGs form and assemble a good portion of their stellar mass at relatively early times (say $z \gtrsim 1$), during the virialization of their host systems. At later times (say $z \lesssim 1$), further growth of the CGs occurs, when their hosts are almost virialized, through galactic cannibalism, that is the accretion of companion galaxies orbiting in the common host dark-matter (DM) halo. Galactic cannibalism, which was originally proposed as the dominant process to form CGs in clusters (Ostriker & Tremaine 1975; White 1976; Hausman & Ostriker 1978), is driven by dynamical friction (Chandrasekhar 1943), so the CGs must accrete preferentially relatively massive satellite galaxies (Ostriker & Tremaine 1975), because the dynamical-friction time-scale is inversely proportional to the mass of the decelerated object. As these accreted satellite galaxies live in the dense environment of the group or cluster core, they are expected to be poor in cold gas and not to have significant ongoing star formation. For these reasons, the growth of CGs by galactic cannibalism should be well represented by a sequence of dissipationless (dry) mergers. This is consistent with the observational finding that CGs are invariably ETGs. The cumulative effect of these accretion episodes is important in the build-up of these massive galaxies: both observational (Marchesini et al. 2014; Buchan & Shankar 2016; Bellstedt et al. 2016; Vulcani et al. 2016b) and theoretical (De Lucia & Blaizot 2007; Tonini et al. 2012; Shankar et al. 2015) studies suggest that the stellar mass of CGs in clusters of galaxies has grown by up to a factor of 2 since $z \approx 1$. Similar growth rates are found in simulations of group CG formation (Feldmann et al. 2010).

CGs are observed to follow relatively tight empirical scaling laws, relating stellar mass (or luminosity), size and stellar velocity dispersion (Bernardi et al. 2007; Liu et al. 2008; Vulcani et al. 2014). There are indications that these scaling relations are even tighter than those of normal ETGs (Bernardi et al. 2007; Montero-Dorta et al. 2016). If the idea that CGs grow significantly via galactic cannibalism is correct, the high-mass end of the ETG scaling relations must be built and maintained by dry mergers (Nipoti et al. 2003b; Bernardi et al. 2011), which are known to have an impact on the scaling laws (Nipoti, Londrillo & Ciotti 2003a; Boylan-Kolchin, Ma & Quataert 2005). The effect of the accretion of a satellite on the size and velocity dispersion depends not only on the properties of the satellite (such as mass and velocity dispersion; Naab, Johansson & Ostriker 2009), but also on the orbital parameters of the encounter (Boylan-Kolchin, Ma & Quataert 2006; Nipoti et al. 2012). In cosmologically motivated simulations of formation

★ E-mail: carlo.nipoti@unibo.it

of brightest group galaxies (Taranu, Dubinski & Yee 2013, 2015; Perea & Solanes 2016; Solanes et al. 2016), the final CGs, though forming through complex merger histories, are found to follow tight scaling relations, similar to those observed for the real CGs. The knowledge of the distribution of the merging orbital parameters could help understand this finding.

In this paper, we focus on the late cannibalism-driven growth of CGs and we explore the properties of the central-satellite encounters. The orbital parameters of these encounters are expected to be mainly determined by the fact that each CG is located in a very special place, that is the bottom of the deep gravitational potential well of a group or cluster of galaxies. Mutatis mutandis, the process of the accretion of satellites on to a CG is very similar to the process of the formation of galactic stellar nuclei via accretion of galactic globular clusters (Gnedin & Ostriker 1997; Gnedin, Ostriker & Tremaine 2014). In essence, the idea is that the satellite galaxies that end up being cannibalized by the CG not only span a relatively small range in mass (they must be massive enough for dynamical friction to be effective), but also have a special distribution of the orbital parameters at the time of encounter with the CG (because their orbits are determined mainly by dynamical friction). In the attempt to better characterize the properties of the central-satellite encounters in groups and clusters, in this work, we follow with *N*-body simulations the evolution of the orbital energy and angular momentum of model group and cluster satellite galaxies under the effect of dynamical friction against the cluster DM halo. These simulations allow us to determine the distributions of the orbital parameters of the central-satellite encounters. We then compare these distributions, relevant to the growth of CGs in groups and clusters, to the distributions of the orbital parameters measured for infalling satellite haloes in cosmological *N*-body simulations, which are expected to describe accretion on to galaxies that are not centrals in either groups or clusters.

The paper is organized as follows. The models and the *N*-body simulations are described in Sections 2 and 3, respectively. The results on the distributions of the orbital parameters are presented in Section 4 and discussed in Section 5. Section 6 concludes.

2 MODELS AND PHYSICAL UNITS

We study the growth of CGs with the help of idealized models. The accretion of satellites occurs on time-scales of the order of the dynamical-friction time-scale, which is longer than the violent-relaxation time-scale (Lynden-Bell 1967), that is the characteristic time for the virialization of the host halo. Therefore, the satellite galaxies accreted by the CGs are not expected to be directly traced by the population of infalling cosmological sub-haloes at their first pericentric passage, but to belong to a population of satellites roughly in equilibrium in the gravitational potential of the host halo (see Section 5.1 for a discussion). Therefore, we simply assume that in the initial conditions the halo is in equilibrium and the satellite galaxies are on orbits extracted from the halo distribution function. Of course, the distribution function of the satellites must not necessarily be the same as that of the host DM halo, but the two distributions are expected to be similar, because they both originate from cosmological accretion. This is supported by the analysis of haloes in cosmological *N*-body simulations, in which DM particles and sub-haloes are found to have similar velocity distribution (Diemand, Moore & Stadel 2004; Gill et al. 2004).

Specifically, in our model the halo is represented by a spherical, exponentially truncated Navarro, Frenk & White (1996, hereafter NFW) density distribution:

$$\rho(r) = \frac{M_{\rm ref}}{r\,(r+r_{\rm s})^2}\exp\left[-\left(\frac{r}{r_{\rm t}}\right)^2\right], \tag{1}$$

where $r_{\rm s}$ is the scale radius, $r_{\rm t}$ is the characteristic radius of the exponential truncation and $M_{\rm ref}$ is a reference mass. We fix $r_{\rm t}=5r_{\rm s}$, so the total DM mass is $M_{\rm tot}=4\pi\int_0^\infty \rho r^2{\rm d}r \simeq 0.82M_{\rm ref}$. The halo is assumed to have Osipkov–Merritt (Osipkov 1979; Merritt 1985) distribution function:

$$f(Q) = \frac{1}{\sqrt{8}\pi^2}\frac{\rm d}{{\rm d}Q}\int_Q^0 \frac{{\rm d}\rho_{\rm a}}{{\rm d}\Phi}\frac{{\rm d}\Phi}{\sqrt{\Phi-Q}}, \tag{2}$$

where $Q=E+L^2/2r_{\rm a}^2$, E is the specific energy, L is the specific angular-momentum modulus and Φ is the gravitational potential, such that

$$\nabla^2\Phi = 4\pi G\rho, \tag{3}$$

where ρ is the density distribution (equation 1). In equation (2),

$$\rho_{\rm a}(r) \equiv \left(1+\frac{r^2}{r_{\rm a}^2}\right)\rho(r) \tag{4}$$

is the so-called augmented density, where $r_{\rm a}$ is the anisotropy radius. The Osipkov–Merritt distribution function is such that the velocity distribution is isotropic for $r_{\rm a}/r_{\rm s}=\infty$ and increasingly radially anisotropic for smaller values of $r_{\rm a}/r_{\rm s}$. For fixed $r_{\rm a}/r_{\rm s}$, the velocity distribution is isotropic in the system's centre and more and more radially biased for increasing distance from the centre.

For simplicity, the satellite is modelled as a 'rigid' (i.e. represented by a single particle) system of mass $M_{\rm sat}$ orbiting in the 'live' (i.e. represented by an *N*-body system) distribution of the halo (see Section 5.2 for a discussion of this assumption). The CG is not modelled explicitly, but the central mass distribution of the host can be thought of as due to the CG. Therefore, we define as fiducial radius of the CG $r_{\rm cen}=0.12r_{\rm s}$ and as fiducial mass of the CG

$$M_{\rm cen} = M(r_{\rm cen}) \simeq 0.0075M_{\rm tot}, \tag{5}$$

where $M(r)=4\pi\int_0^r\rho r^2{\rm d}r$ with $\rho(r)$ given by equation (1). The characteristic velocity dispersion of the CG is $\sigma_{\rm cen}\equiv\sqrt{GM_{\rm cen}/r_{\rm cen}}$. The specific choice of the value of $r_{\rm cen}/r_{\rm s}$ is somewhat arbitrary: As long as the mass ratio $M_{\rm cen}/M_{\rm tot}$ between the central galaxy and the host halo is realistic, other values of $r_{\rm cen}/r_{\rm s}$ would be equally well motivated. However, we verified that the main results of the present work are not sensitive to the specific choice of $r_{\rm cen}/r_{\rm s}$, at least for values in the range $0.1\lesssim r_{\rm cen}/r_{\rm s}\lesssim 0.15$ (corresponding to mass ratios $0.005\lesssim M_{\rm cen}/M_{\rm tot}\lesssim 0.011$).

The model can be rescaled by choosing the mass unit $M_{\rm tot}$ and the length unit $r_{\rm s}$. The corresponding units for other physical quantities are the velocity unit

$$v_{\rm u}\equiv\sqrt{\frac{GM_{\rm tot}}{r_{\rm s}}} \simeq 2074\left(\frac{M_{\rm tot}}{10^{14}\,{\rm M}_\odot}\right)^{1/2}\left(\frac{r_{\rm s}}{100\,{\rm kpc}}\right)^{-1/2}{\rm km\,s^{-1}}, \tag{6}$$

the time unit

$$t_{\rm u}\equiv\sqrt{\frac{r_{\rm s}^3}{GM_{\rm tot}}} \simeq 4.72\times10^7\left(\frac{r_{\rm s}}{100\,{\rm kpc}}\right)^{3/2}\left(\frac{M_{\rm tot}}{10^{14}\,{\rm M}_\odot}\right)^{-1/2}{\rm yr}, \tag{7}$$

the specific-energy unit $E_u \equiv v_u^2$ and the specific angular-momentum unit $L_u \equiv r_s v_u$. It follows that, for instance, for a system with $M_{tot} = 10^{14}\,M_\odot$ and $r_s = 200$ kpc, the characteristic mass, size and velocity dispersion of the central galaxy are, respectively, $M_{cen} \simeq 7.5 \times 10^{11}\,M_\odot$, $r_{cen} \simeq 24$ kpc and $\sigma_{cen} \simeq 367$ km s^{-1}.

3 NUMERICAL EXPERIMENTS

3.1 Set-up of the *N*-body simulations

In each simulation, the initial conditions consist of an equilibrium spherical DM halo with density distribution given by equation (1), realized with $N \simeq 10^6$ particles, hosting a massive particle of mass M_{sat}, representing the satellite. All DM particles have the same mass $m = M_{tot}/N \simeq 10^{-6} M_{tot}$. As we follow the evolution of a single satellite in each simulation, we neglect the effects of satellite–satellite interactions, which, however, are not expected to be very important, as also suggested by studies of the evolution of the sub-halo population in cosmological haloes (van den Bosch & Jiang 2016).

The *N*-body simulations were run with the parallel collisionless code FVFPS (Nipoti et al. 2003a; Londrillo, Nipoti & Ciotti 2003). We adopted the following values of the code parameters: minimum value of the opening parameter $\theta_{min} = 0.5$, softening parameter for the DM particles $\varepsilon_{DM} = 0.02 r_s$ and adaptive time-step Δt (the same for all particles, but varying as a function of the maximum mass density) spanning the range $0.01 \lesssim \Delta t/t_u \lesssim 0.1$.

We explore four different families of models obtained by combining two values of the anisotropy parameter r_a and two values of the satellite mass M_{sat}. In particular, we explored an isotropic model ($r_a/r_s = \infty$) and a radially anisotropic model ($r_a/r_s = 2$): These two models should bracket the range in orbital anisotropy for group and cluster-scale DM haloes, which are expected to have moderately radially biased orbits (Ascasibar & Gottlöber 2008; Wojtak, Gottlöber & Klypin 2013). For each choice of r_a, we explored two values of the satellite mass: $\mu_{sat} = 0.001$ and 0.005, where $\mu_{sat} \equiv M_{sat}/M_{tot}$ is the satellite mass in units of the total mass of the host. So, given our definition of the CG mass (equation 5), the mass ratio between the satellite and the central is $M_{sat}/M_{cen} \simeq 0.133$ when $\mu_{sat} = 0.001$ and $M_{sat}/M_{cen} \simeq 0.667$ when $\mu_{sat} = 0.005$. In the simulations, the particle representing the satellite has softening length ε_{sat}, depending on the satellite mass M_{sat}: $\varepsilon_{sat} = 0.05 r_s$ when $\mu_{sat} = 0.001$ and $\varepsilon_{sat} = 0.08 r_s$ when $\mu_{sat} = 0.005$. The simulations are run for a maximum time $t_{max} = 200 t_u$. We verified numerically that the anisotropic model is stable by running it without the massive satellite for $200 t_u$.

For given initial orbital parameters E_0 and L_0, at $t = 0$ the satellite is placed at the apocentre of the orbit: Taking as reference a Cartesian system with origin in the halo centre, the initial coordinates of the satellites are $y = r_{apo}$, $v_x = v_{apo}$, $x = z = v_y = v_z = 0$, where r_{apo} is the apocentric radius and $v_{apo} = \sqrt{2[E_0 - \Phi(r_{apo})]}$. If the satellite had the same mass as the DM particles ($M_{sat} = m$) it would orbit in the stationary potential with constant specific energy $E(t) = E_0$ and angular momentum $L(t) = L_0$. We ran a few test simulations with $M_{sat} = m$ (and $\varepsilon_{sat} = \varepsilon_{DM} = 0.02 r_s$) finding that E and L are conserved to within 0.5 per cent and 5 per cent, respectively, over the time span of $200 t_u$.

3.2 Definition of the final time and classification of the runs

In the simulations, the ratio between satellite mass and DM particle mass ($M_{sat}/m = 1$–5×10^3) is sufficiently large to fully catch the effect of dynamical friction. The satellite tends to spiral-in towards the centre of the halo, losing angular momentum (L decreases) and becoming more bound to the host system (E decreases). We monitor the orbit of the satellite and, in particular, we measure as a function of time the distance $d = \sqrt{x^2 + y^2 + z^2}$ of the satellite from the halo centre. In all cases, in the initial conditions $d > r_{cen}$, where r_{cen} is the fiducial radius of the CG (Section 2). We define the *final time* of the simulation t_{fin} as the time when the satellite first crosses the sphere of radius r_{cen} centred in the halo centre of mass. If this occurs before t_{max}, we classify the run as an *encounter* (either *merger* or *fly-by*; see Section 4.3) between the satellite and the CG. When the encounter does not occur before t_{max}, the run is excluded from further analysis, because the satellite is not likely to contribute to accretion on to the CG (we note that, for instance, $t_{max} = 200 t_u \approx 10^{10}$ yr when $r_s = 100$ kpc and $M_{tot} = 10^{14}\,M_\odot$; see equation 7).

3.3 Properties of the families of simulations

For $\mu_{sat} = 0.005$, we ran 34 simulations with $r_a/r_s = \infty$ (family I5) and 34 simulations with $r_a/r_s = 2$ (family A5). In each of these 68 simulations, the initial orbit of the satellite is chosen by extracting randomly the initial energy E_0 and angular momentum L_0 from the distribution function (equation 2) of the host halo. As for the DM particles (see Section 3.1), the anisotropy distributions of the satellites in the two considered models (isotropic and radially anisotropic with $r_a/r_s = 2$) should bracket the anisotropy distribution expected for satellite galaxies in clusters (Iannuzzi & Dolag 2012).

Of the aforementioned 68 simulations, those that ended up with an encounter between CG and satellite (24 in the isotropic case, 34 in the anisotropic case) were also rerun with the same initial conditions, but lower satellite mass $\mu_{sat} = 0.001$ (these families of simulations are called I1 and A1, respectively[1]). Of these 58 simulations with $\mu_{sat} = 0.001$, 24 ended up with an encounter (9 in the anisotropic case, 15 in the isotropic case). Thus, altogether we ran 126 simulations, 82 of which ended up with an encounter (see Table 1). The time t_{fin} elapsed before the encounter depends on both the initial orbital parameters and the satellite's mass. The distribution of t_{fin}/t_u for the 82 simulations classified as encounters, shown in Fig. 1, is quite broad, spanning the range $1.3 \lesssim t_{fin}/t_u \lesssim 190$, with mean $\simeq 78$ and standard deviation $\simeq 54$.

4 RESULTS

4.1 Morphology of the orbits

Two examples of the trajectories of simulations in which the satellite spirals-in down to the CG are shown in the top panels of Fig. 2. For the same two simulations, the bottom panels of Fig. 2 show the distance d of the satellite from the halo centre as a function of time. The DM phase-space distribution (equation 2 with $r_a/r_s = \infty$) and the initial conditions of the satellite's orbit are the same in the two simulations, which differ only for the value of μ_{sat}. These plots nicely show that, as well known, dynamical friction is more effective when $\mu_{sat} = 0.005$ than when $\mu_{sat} = 0.001$. The final time of the simulation t_{fin}, such that $d(t_{fin}) = r_{cen}$, is $t_{fin}/t_u \simeq 190$ when $\mu_{sat} = 0.001$ and $t_{fin}/t_u \simeq 50$ when $\mu_{sat} = 0.005$.

[1] The 10 simulations with $\mu_{sat} = 0.005$ that did not end up with an encounter were not rerun with $\mu_{sat} = 0.001$, because we know in advance that the encounter would not occur for $\mu_{sat} = 0.001$, because dynamical friction is less effective for a lower mass satellite.

Table 1. Properties of the four families of models (I1, I5, A1, A5). $\mu_{\rm sat} = M_{\rm sat}/M_{\rm tot}$: mass of the satellite in units of the total mass of the host system. $r_{\rm a}/r_{\rm s}$: ratio between the anisotropy radius and the scale radius of the host halo. Runs: number of simulations. Encounters: number of runs that ended up with an encounter (as defined in Section 3.2). Mergers: number of encounters classified as bona-fide mergers. Fly-bys: number of encounters classified as fly-bys (Section 4.3.1).

Family	$\mu_{\rm sat}$	$r_{\rm a}/r_{\rm s}$	Runs	Encounters	Mergers	Fly-bys
I1	0.001	∞	24	15	7	8
I5	0.005	∞	34	24	19	5
A1	0.001	2	34	9	3	6
A5	0.005	2	34	34	16	18

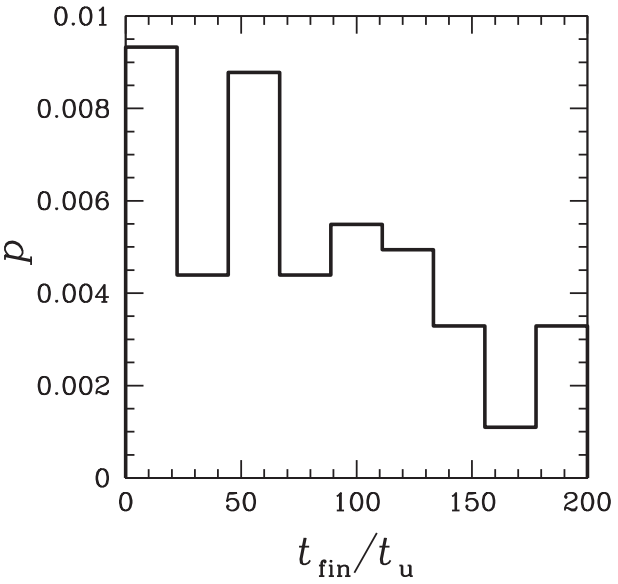

Figure 1. Probability distribution $p = {\rm d}n/{\rm d}x$ of the final time $t_{\rm fin}$ defined in Section 3.2 ($x = t_{\rm fin}/t_{\rm u}$, where $t_{\rm u}$ is the time unit; see Section 2) for the simulations classified as encounters.

4.2 Evolution of energy and angular momentum

4.2.1 Lindblad diagrams

The effect of dynamical friction can be quantitatively visualized in the so-called *Lindblad diagram* (Lindblad 1933), which is a representation of the evolution of the orbits in the E–L space. It is useful to define the maximum specific angular-momentum modulus for an orbit with specific energy E, which is the specific angular-momentum modulus $L_{\rm circ}$ of the circular orbit with the same specific energy. The curve $L_{\rm circ}(E)$ delimits the allowed region $L(E) \leq L_{\rm circ}(E)$ in the Lindblad diagram. Given a spherical gravitational potential, due to dynamical friction a massive particle (such as the satellite considered in our model) is expected, in the Lindblad diagram, to follow tracks in the direction of decreasing specific energy and angular momentum (Tremaine, Ostriker & Spitzer 1975). The rate of evolution along the track increases with the satellite mass (in the limit $M_{\rm sat} = m$ the rate becomes zero because E and L are integrals of motion). Such tracks are found numerically in our N-body simulations, as apparent from the panels in Fig. 3, showing the initial position, final position and trajectory of the satellite in the E–L plane for the subset of runs that ended up with an encounter between the satellite and the CG. We note that the trajectories are smoother for more massive satellites ($\mu_{\rm sat} = 0.005$; right-hand panels in Fig. 3) than for less massive satellites ($\mu_{\rm sat} = 0.001$; left-hand panels in Fig. 3). Fig. 3 also shows that, at the final time $t_{\rm fin}$, the satellites are confined in the bottom area of the E–L plane: In fact, as we define $t_{\rm fin}$ as the time when the satellite is at a distance $r_{\rm cen}$ from the centre (Section 3.2), for given final E there is an upper limit on the final L (see Section 4.2.3).

4.2.2 Orbit circularization?

A long-standing question is whether dynamical friction tends to circularize the orbit of the decelerated object (e.g. Hashimoto, Funato & Makino 2003). Our simulations can provide useful information to address this question. In Fig. 3, circular orbits lie on the dashed curves: Therefore, the effect of circularization would be to bring the orbits closer to these curves. The numerical tracks in the plots run typically 'parallel' to these curves, so there is no clear evidence of circularization.

A quantitative measure of the deviation from circular orbit is the pericentric-to-apocentric radius ratio $r_{\rm peri}/r_{\rm apo}$, which is unity for circular orbits and $\ll 1$ for very eccentric orbits. At any given time t in our simulations, we define $r_{\rm peri}$ and $r_{\rm apo}$ of the satellite as the pericentric and apocentric radii of an orbit with constant specific energy E and angular momentum L, where E and L are those measured at time t. The evolution of the pericentric-to-apocentric radius ratio in our simulations can be inferred from Fig. 4, which plots the final ($t = t_{\rm fin}$) ratio $r_{\rm peri}/r_{\rm apo}$ as a function of the initial ($t = 0$) ratio $r_{\rm peri}/r_{\rm apo}$. In the plot, the diagonal line corresponds to no net evolution in $r_{\rm peri}/r_{\rm apo}$: If a point lies above (below) this line, the corresponding final orbit is more circular (eccentric) than the initial orbit. Overall, the distribution of points in Fig. 4 does not suggest that dynamical friction leads to orbit circularization. In most cases, especially for the lower mass satellites with $\mu_{\rm sat} = 0.001$, the final and initial ratios, $r_{\rm peri}/r_{\rm apo}$, are very similar. In some simulations with $\mu_{\rm sat} = 0.005$, the final $r_{\rm peri}/r_{\rm apo}$ is significantly different from the initial value, but in most of these cases, the final orbit is more eccentric than the initial orbit.

Broadly speaking, our results are in agreement with previous studies, suggesting that the effect of dynamical friction is not necessarily orbit circularization. For instance, van den Bosch et al. (1999) found that $r_{\rm peri}/r_{\rm apo}$ does not evolve significantly for a massive satellite orbiting in a truncated isothermal halo. The trend observed in Fig. 3 is similar to that found by Arena & Bertin (2007) in analogous numerical experiments, but with stellar systems with different distribution functions. Arena & Bertin (2007) conclude that, though in some cases the effect of dynamical friction is to circularize the orbit (see also Bontekoe & van Albada 1987), this is not a general result, and that the orbital evolution depends on the properties of the host stellar system. We do not find evidence of significantly different evolution of $r_{\rm peri}/r_{\rm apo}$ in simulations with anisotropic (A1 and A5) and isotropic (I1 and I5) distribution functions, as instead found by Casertano, Phinney & Villumsen (1987) and Tsuchiya & Shimada (2000), who however studied different families of stellar systems. Moreover, it must be stressed that, unlike Casertano et al.

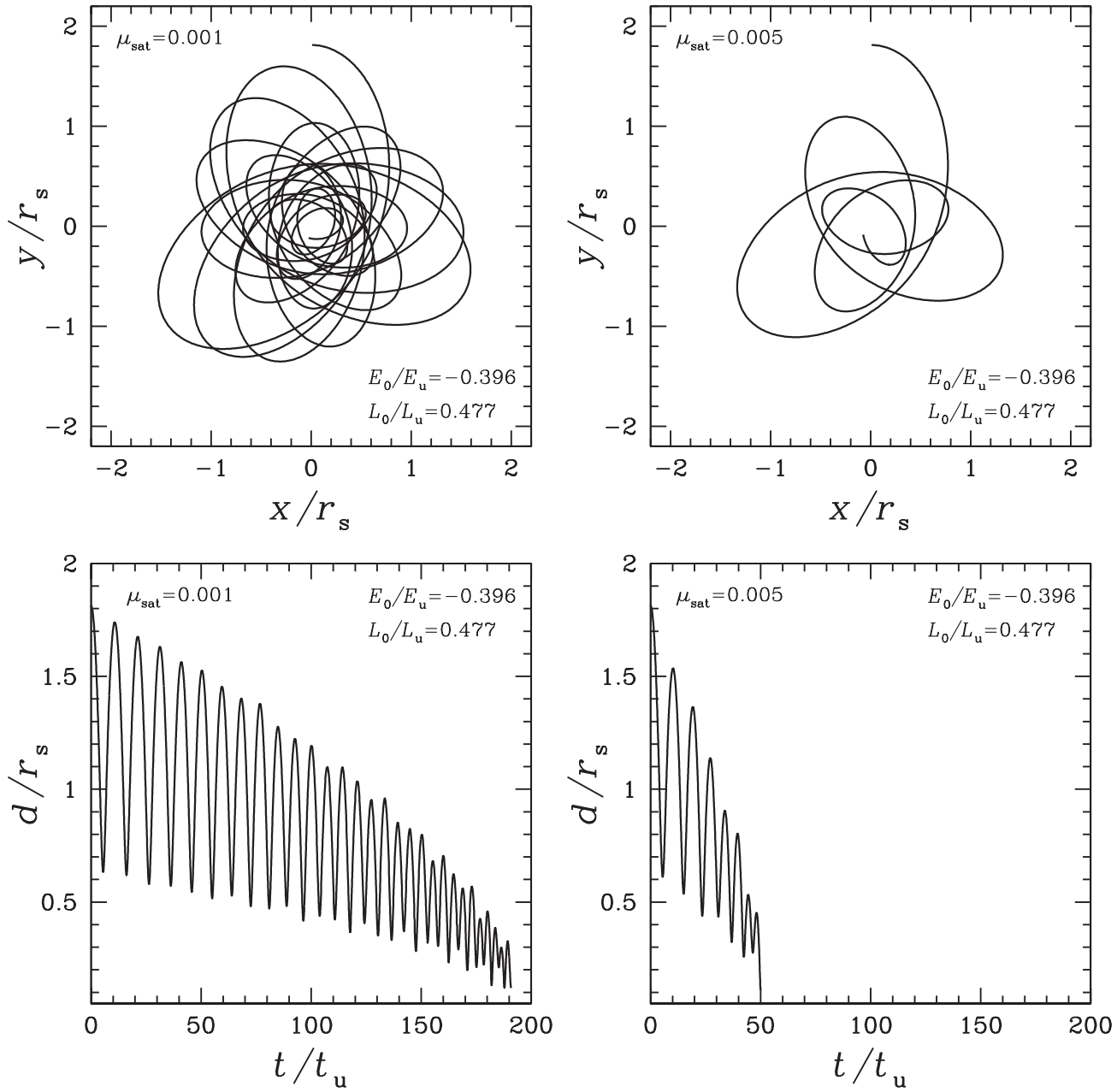

Figure 2. Upper panels: trajectories of the satellite in the x–y plane in two representative simulations with the same (isotropic; $r_a/r_s = \infty$) DM phase-space distribution and initial satellite's orbital parameters (E_0, L_0), but different satellite's mass: $\mu_{sat} = 0.001$ (left-hand panel) and $\mu_{sat} = 0.005$ (right-hand panel). The trajectories are drawn from $t = 0$ ($x = 0$, $y = d \simeq 1.8r_s$) to the final time t_{fin} when the satellite crosses the central sphere of radius $r_{cen} = 0.12r_s$. Lower panels: distance d of the satellite from the centre of the host halo as a function of time for the same two simulations as in the upper panels: $\mu_{sat} = 0.001$ (left-hand panel) and $\mu_{sat} = 0.005$ (right-hand panel). $d(t)$ is drawn from $t = 0$ to the final time t_{fin}, such that $d(t_{fin}) = r_{cen} = 0.12r_s$. Here r_s is the halo scale radius, t_u is the time unit, L_u is the specific angular-momentum unit and E_u is the specific energy unit (see Section 2).

(1987) and Tsuchiya & Shimada (2000), in our experiments we are not comparing the evolution of orbits with the same initial orbital parameters in isotropic and radially anisotropic host systems, because in our simulations the initial orbital parameters of the satellite are extracted from the same distribution function as that of the host halo (see Section 2). As suggested by Statler (1991), the host system tries to make the satellites conform to its orbital structure, consistent with the fact that in our simulations there is not a net trend towards orbit circularization, in either the isotropic or the anisotropic case.

In summary, the results of our simulations add further evidence that dynamical friction does not necessarily lead to orbit circularization: The effect on the orbit of the decelerated object depends not only on the host's distribution function, but also, for given distribution function, on the initial orbital parameters of the satellite.

4.2.3 Final specific energy and angular momentum

The final ($t = t_{fin}$) positions of the satellites in the E–L diagram are shown in Fig. 5. We recall that, by definition, these final points are such that the distance of the satellite from the centre is $d = r_{cen}$.

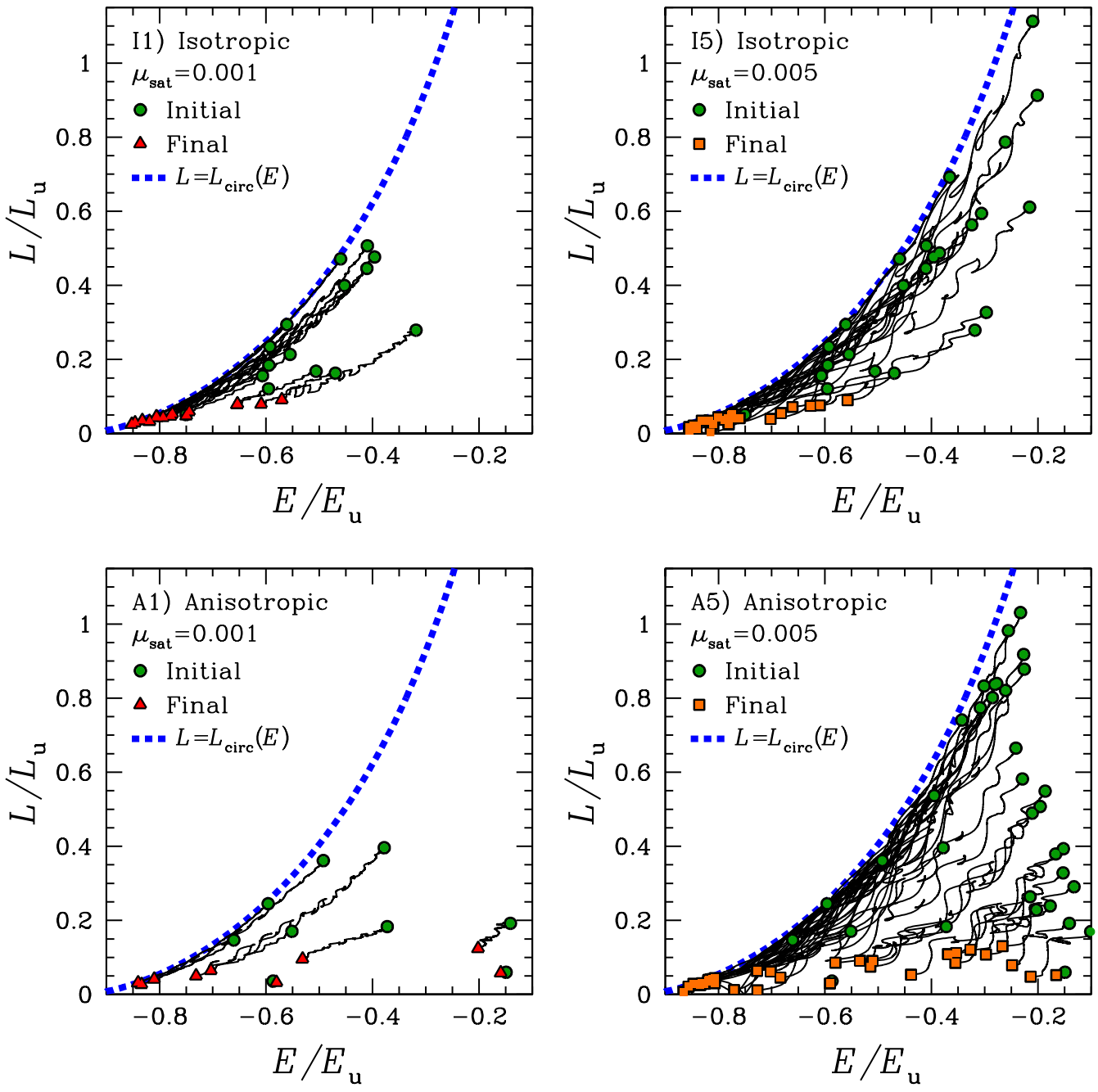

Figure 3. Initial ($t = 0$; circles) and final ($t = t_{fin}$; triangles and squares) specific angular-momentum modulus L versus specific energy E of the satellite in the families of models I1, I5, A1 and A5 (from top left to bottom right). Only runs that ended up with an encounter between the CG and the satellite are plotted. The thin solid curves indicate the trajectories of the satellite in the E–L space. The thick dashed curve indicates the specific angular-momentum modulus of a circular orbit with specific energy E. Here E_u and L_u are, respectively, the specific energy and angular-momentum units of the model (see Section 2).

At fixed position and energy of the satellite, the maximum allowed specific angular momentum is in general smaller than L_{circ}. For given distance from the centre of the host halo d and given specific energy E, the maximum value of L is

$$L_{max} = d\sqrt{2[E - \Phi(d)]} = dv, \quad (8)$$

where v is the speed of the satellite when it is at a distance d from the centre. Clearly, $L_{max} \leq L_{circ}(E)$ and L_{max} is such that $L/L_{max} = v_{tan}/v$, where v_{tan} is the tangential velocity.

From Fig. 5 it is apparent that the allowed region in the final E–L space is not uniformly populated, but the points tend to cluster close to the maximum value L_{max}. This suggests that when the satellite encounters the CG it preferentially has almost the maximum angular momentum allowed for its energy. We have seen in Section 4.2.2 that dynamical friction does not always tend to circularize the orbit and that, in any case, the effect of dynamical friction on the orbital eccentricity is typically small (see Fig. 4). The fact that the final L is often close to L_{max} is not due to orbit circularization, but to the fact that, given the small size of the CG compared to the host system, it is more likely that the encounter happens on an orbit 'grazing' the CG than on a very radial orbit penetrating the CG close to the centre. This is due to the fact that only a small fraction of the system's

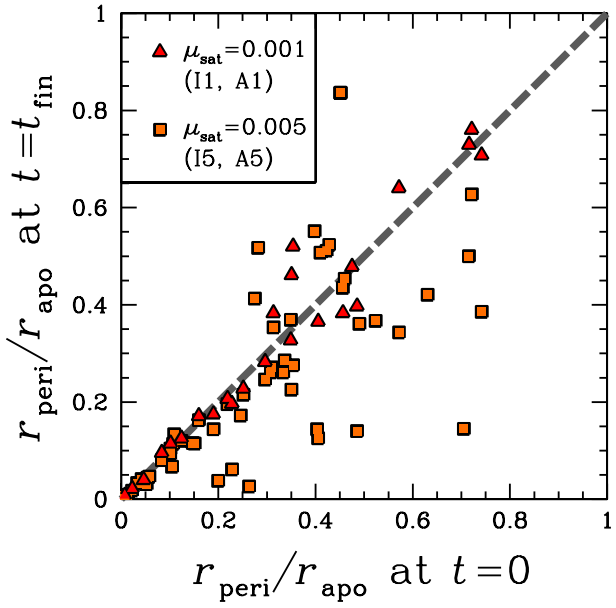

Figure 4. Final versus initial pericentric-to-apocentric radius ratio $r_{\rm peri}/r_{\rm apo}$ of the satellite's orbit for simulations that ended up with an encounter. The diagonal dashed line indicates no net evolution in $r_{\rm peri}/r_{\rm apo}$.

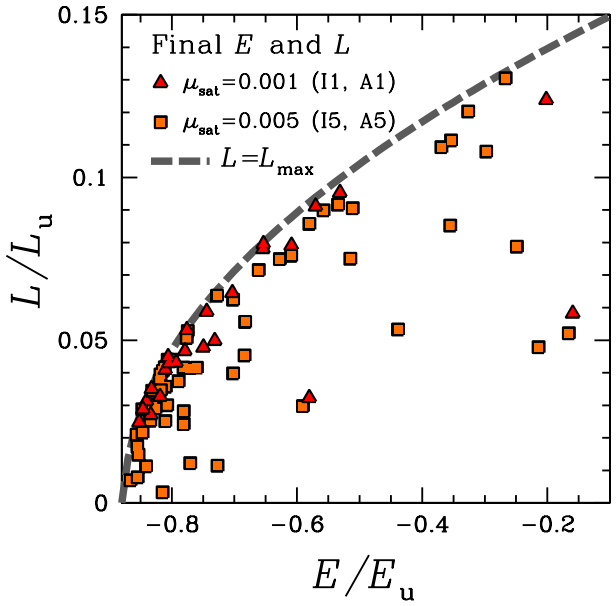

Figure 5. Final ($t = t_{\rm fin}$, $d = r_{\rm cen}$) specific angular-momentum modulus L versus specific energy E of the satellite in the same units as in Fig. 3. The thick long-dashed curve indicates the maximum specific angular-momentum modulus $L_{\rm max}$ of a particle with specific energy E located at a distance $d = r_{\rm cen}$ from the halo centre (equation 8).

orbits go directly through the host's core. The majority of orbits are less eccentric and shrink as a consequence of dynamical friction, leading to almost tangential encounters between the satellite and the CG.

4.3 Central-satellite orbital parameters in the two-body approximation

When an encounter between the central and the satellite occurs it is useful to describe it in terms of the orbital parameters calculated in the point-mass two-body approximation. This formalism, though not rigorous for extended objects, is often used in the study and classification of mergers of galaxies (e.g. Boylan-Kolchin et al. 2006; Nipoti, Treu & Bolton 2009) and DM haloes (e.g. Khochfar & Burkert 2006; Posti et al. 2014).

From the point of view of the central-satellite galaxy orbit, we define the two-body approximation orbital energy per unit mass

$$E_{\rm 2b} = \frac{1}{2}v^2 - \frac{GM_{\rm 2b}}{d}, \tag{9}$$

where $M_{\rm 2b} \equiv M_{\rm cen} + M_{\rm sat}$, d is the relative distance and v is the relative speed. As the CG is at rest in the centre of the halo, d and v are, respectively, the distance and the speed of the satellite relative to the halo centre. Therefore, the specific orbital angular momentum per unit mass is just the specific angular momentum of the satellite, with modulus $L = dv_{\rm tan}$.

In the two-body approximation, the orbit can be characterized also by different combinations of the two parameters $E_{\rm 2b}$ and L. In particular, it is useful to define the eccentricity

$$e = \sqrt{1 + \frac{2E_{\rm 2b}L^2}{G^2M_{\rm 2b}^2}} \tag{10}$$

and the pericentric radius

$$r_{\rm peri,2b} = \frac{GM_{\rm 2b}}{2E_{\rm 2b}}(e-1). \tag{11}$$

For bound orbits ($E_{\rm 2b} < 0$, i.e. $e < 1$) we also define the circularity

$$\eta = \sqrt{1-e^2}. \tag{12}$$

4.3.1 *Bona-fide mergers and fly-bys*

Not in all the runs that ended up with an encounter, we expect to have a rapid merger between the central and the satellite galaxies. Rapid mergers occur when the orbits are bound $E_{\rm 2b} < 0$, but also for unbound orbits ($E_{\rm 2b} \geq 0$), provided the orbital angular-momentum modulus L is sufficiently low (see section 7.4 of Binney & Tremaine 1987). For this reason, a convenient parameter that can be used to identify rapid mergers is the eccentricity e, which, for $E_{\rm 2b} > 0$, is an increasing function of both $E_{\rm 2b}$ and L. We take as fiducial discriminating value of eccentricity $e = 1.5$ and classify an encounter as a *bona-fide merger* when $e < 1.5$ and as a *fly-by* when $e > 1.5$. The distribution of e for our runs that ended up with an encounter is shown in Fig. 6. The distribution of the mergers is characterized by a peak around $e = 1$. A substantial fraction of the fly-bys has very high eccentricity (up to $e \gtrsim 10$): In these cases the satellite, though bound to the deep potential well of the host DM halo, appears as highly unbound from the point of view of the central-satellite interaction.

Fig. 7 plots the final position of the satellites in the $E_{\rm 2b}$–L plane. Similar to Fig. 5, also in this case, the separation d between central and satellite is fixed $d = r_{\rm cen}$, so the allowed region of the $E_{\rm 2b}$–L plane is $L \leq L_{\rm max}$, where $L_{\rm max} = dv$ (equation 8), and v is the satellite's speed when $d = r_{\rm cen}$. Similar to Fig. 5, also in Fig. 7 the points (in particular those representing mergers) tend to cluster close to the curve $L_{\rm max}(E_{\rm 2b})$, indicating high orbital angular momentum for the accreted satellites. The orbital energy for bona-fide mergers is found in the range $-1.5 \lesssim E_{\rm 2b}/\sigma_{\rm cen}^2 \lesssim 1$, where $\sigma_{\rm cen}$ is the characteristic velocity dispersion of the CG (Section 2).

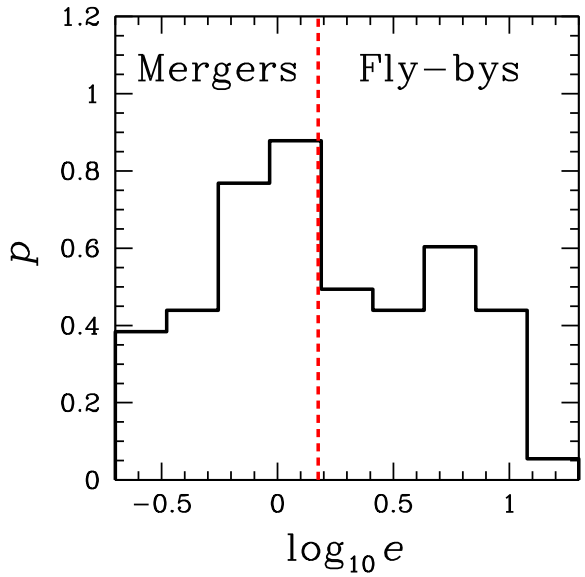

Figure 6. Probability distribution $p = \mathrm{d}n/\mathrm{dlog}_{10}e$ of the final ($t = t_{\rm fin}$, $d = r_{\rm cen}$) eccentricity e of central-satellite encounters. The vertical dashed line ($e = 1.5$) separates *bona-fide* mergers ($e < 1.5$) from fly-bys ($e > 1.5$).

4.4 Distributions of the orbital parameters of the bona-fide mergers

We focus here on the bona-fide mergers as defined and selected in Section 4.3.1, for which we want to measure the distributions of the orbital parameters. The final distributions are expected to depend on both the mass of the satellite and on the initial distribution function. However, Fig. 7 suggests that, in particular for mergers, the location in the E_{2b}–L space at $t = t_{\rm fin}$ is not very different for $\mu_{\rm sat} = 0.001$ and 0.005. Moreover, there is not compelling evidence that the final distributions of E_{2b} and L are different in the isotropic and radially anisotropic cases (see Appendix A). Therefore, in order to have a better statistics, hereafter we consider the distributions of the final orbital parameters of all bona-fide mergers, putting together all families of models (I1, I5, A1 and A5).

4.4.1 Distributions of specific energy and angular momentum

The distributions of final E_{2b} and L is shown in Fig. 8: Most orbits are moderately bound ($-1 \lesssim E_{2b}/\sigma^2_{\rm cen} \lesssim 0$) and almost tangential ($L/L_{\rm max} \gtrsim 0.7$). The distribution of $E_{2b}/\sigma^2_{\rm cen}$ is well represented by a Gaussian with mean $\mu = -0.56$ and standard deviation $\sigma = 0.50$. Given that, by definition, $0 \leq L/L_{\rm max} \leq 1$, we attempt to describe the distribution of $L/L_{\rm max}$ with a beta distribution, a natural candidate for continuous random variables with compact support. The probability density function of the beta distribution is

$$p(x) = \frac{x^{\alpha-1}(1-x)^{\beta-1}}{B(\alpha,\beta)}, \tag{13}$$

where

$$B(\alpha,\beta) = \frac{\Gamma(\alpha)\Gamma(\beta)}{\Gamma(\alpha+\beta)} \tag{14}$$

and Γ is the gamma function. We find a good fit to the distribution of $L/L_{\rm max}$ with $\alpha = 1.54$ and $\beta = 0.49$ (for these values the distribution has[2] mean $\mu = 0.76$ and standard deviation $\sigma = 0.25$). The best-fitting Gaussian and beta distributions are overplotted in Fig. 8.

4.4.2 Distributions of eccentricity and pericentric radius

For comparison with work on the orbital parameters of mergers between haloes in cosmological N-body simulations, it is also useful to consider the distribution of the orbital circularity η and pericentric radius $r_{\rm peri,\,2b}$ (see Section 4.3). As η is defined only for bound orbits, we restrict here our analysis to the subsample of our simulations in which the encounter has $e < 1$ (elliptic mergers). The distributions of η and $r_{\rm peri,\,2b}$ are shown in Fig. 9. The distribution of η found for our central-satellite mergers has mean $\mu \simeq 0.64$ and standard deviation $\sigma \simeq 0.28$, and is well represented by a beta distribution (equation 13) with $\alpha = 1.23$ and $\beta = 0.70$. The distribution of $r_{\rm peri,\,2b}/r_{\rm cen}$ has mean $\mu \simeq 0.50$ and standard deviation $\sigma \simeq 0.32$, and appears consistent with being uniform.

The distributions of η and $r_{\rm peri,\,2b}$ that we find for accretion on to CGs are remarkably different from the distributions found for cosmological DM haloes by Wetzel (2011, see Fig. 9). Note that Wetzel (2011) normalizes $r_{\rm peri,\,2b}$ to the virial radius, while here we normalize to $r_{\rm cen}$. However, the right-hand panel of Fig. 9 clearly shows that, independent of the somewhat arbitrary normalization of the x-axis, the shape of the distribution of $r_{\rm peri,\,2b}$ that we find for CGs is different from what was found for DM haloes. In particular, the distribution of η for haloes shown in the left-hand panel of Fig. 9 has mean $\mu \simeq 0.51$ and standard deviation $\sigma \simeq 0.22$, while the distribution of $r_{\rm peri,\,2b}/r_{\rm cen}$ for haloes (right-hand panel of Fig. 9) has mean $\mu \simeq 0.24$ and standard deviation $\sigma \simeq 0.22$.

4.4.3 Distributions of $v/v_{\rm circ}$ and $|v_r|/v$

Another set of orbital parameters often used in the context of cosmological N-body simulations (e.g. Benson 2005; Jiang et al. 2015) is $(v/v_{\rm circ}, |v_r|/v)$ where, given a distance r from the centre of the host system (typically the virial radius), v is the speed of the satellite at r, v_r is the radial component of the satellite velocity at r and $v_{\rm circ}$ is the host's circular velocity at r. The final distributions of $v/v_{\rm circ}$ and $|v_r|/v$, measured by taking as reference radius $r_{\rm cen}$, are shown for all bona-fide mergers ($e < 1.5$) of our simulations in Fig. 10. The distribution of $v/v_{\rm circ}$ is fitted by a Gaussian with mean $\mu = 1.39$ and standard deviation $\sigma = 0.35$, while the distribution of $|v_r|/v$ has $\mu \simeq 0.53$ and $\sigma \simeq 0.27$, and is well represented by a uniform distribution. Consistent with the results of η and $r_{\rm peri,\,2b}$, these distributions are significantly different from the corresponding distributions measured for infalling satellite haloes (at the virial radius) in cosmological N-body simulations by Jiang et al. (2015), which are shown in Fig. 10 for comparison. Specifically, the distributions for cosmological haloes shown in Fig. 10 have mean $\mu \simeq 1.24$ and standard deviation $\sigma \simeq 0.15$ for $v/v_{\rm circ}$, and $\mu \simeq 0.79$ and $\sigma \simeq 0.19$ for $|v_r|/v$.

4.4.4 Comparison with cosmological halo–halo mergers

A summary of the first and second moments of the distributions of the orbital parameters (η, $r_{\rm peri,\,2b}/r_{\rm cen}$, $v/v_{\rm circ}$ and $|v_r|/v$) for the

[2] We recall that for a beta distribution $\sigma^2 = \alpha\beta/[(\alpha+\beta)^2(\alpha+\beta+1)]$ and $\mu = \alpha/(\alpha+\beta)$.

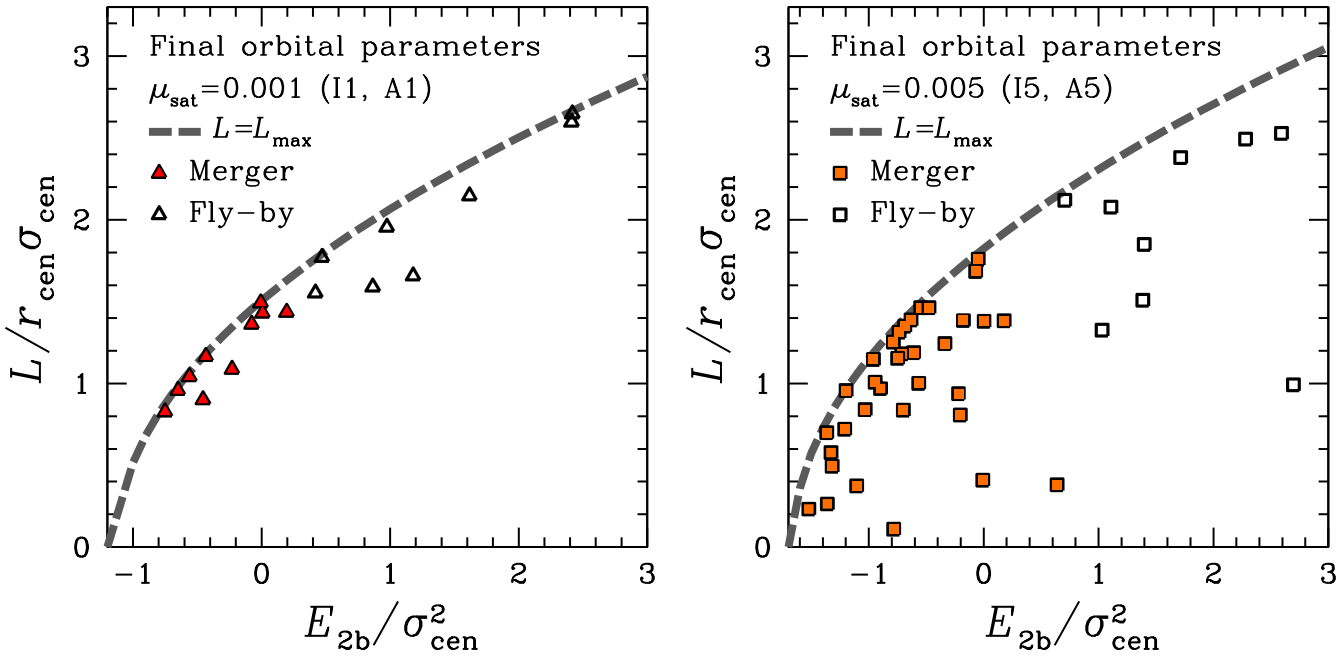

Figure 7. Final ($t = t_{fin}$, $d = r_{cen}$) specific energy (in the two-body approximation) E_{2b} and angular-momentum modulus L of the central-satellite encounter for $\mu_{sat} = 0.001$ (left-hand panel) and $\mu_{sat} = 0.005$ (right-hand panel). Solid symbols represent *bona-fide* mergers, while empty symbols represent fly-bys. The thick long-dashed curve indicates the maximum specific angular-momentum modulus of an encounter with specific energy E_{2b} and satellite-central separation $d = r_{cen}$ (equation 8). Here σ_{cen} and r_{cen} are, respectively, the characteristic velocity dispersion and size of the CG (see Section 2).

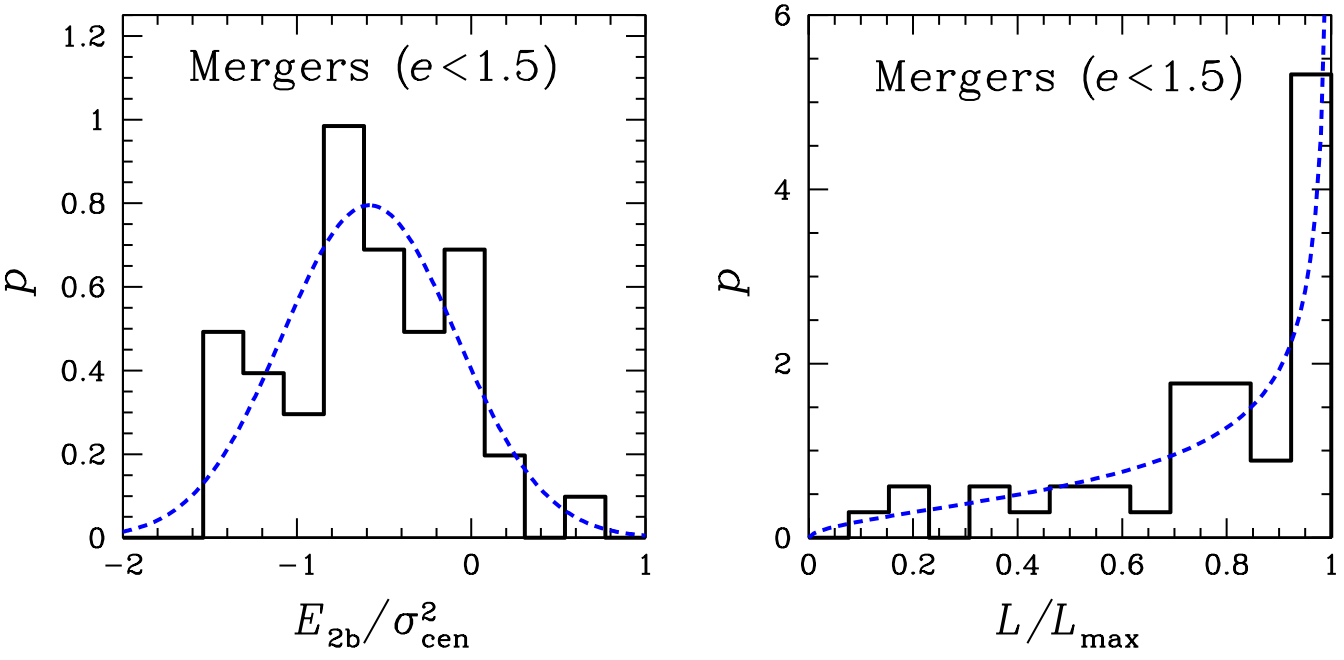

Figure 8. Probability distribution $p = dn/dx$ of the final specific orbital energy, computed in the two-body approximation ($x = E_{2b}/\sigma^2_{cen}$; left-hand panel, solid histogram), and angular-momentum modulus ($x = L/L_{max}$; right-hand panel, solid histogram), where σ_{cen} is the characteristic velocity dispersion of the CG and L_{max} is defined by equation (8). In each panel, the dashed curve represents the analytic best fit of the distribution (see text).

central-satellite mergers of our simulations and for accretion of cosmological satellites is given in Table 2. Based on the results found in this work and in cosmological N-body simulations, we conclude that the probability density functions of the orbital parameters of CG encounters are substantially different from those of the corresponding functions for cosmological haloes. The orbits of satellites merging on to CGs tend to be less bound and less eccentric than the orbits of cosmological satellite haloes when they cross the host's

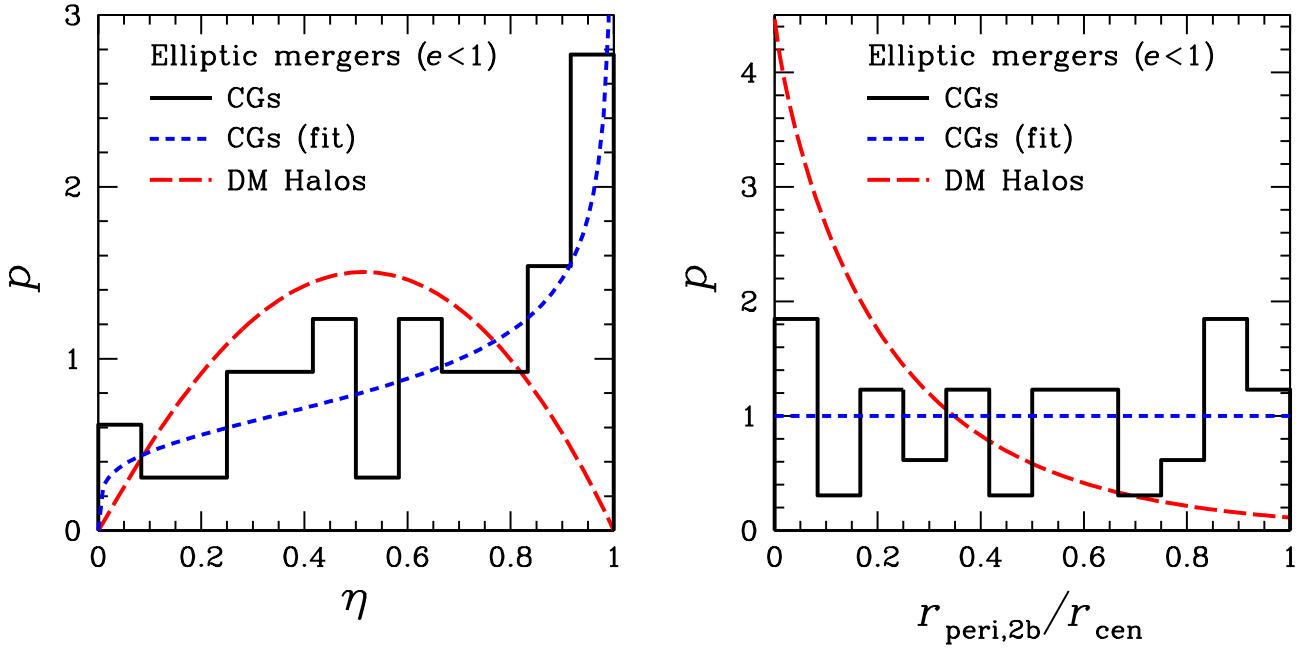

Figure 9. Probability distribution $p = \mathrm{d}n/\mathrm{d}x$ of the final orbital circularity ($x = \eta$; left-hand panel, solid histogram) and pericentric radius ($x = r_{\mathrm{peri,\,2b}}/r_{\mathrm{cen}}$; right-hand panel, solid histogram) for elliptic mergers in the simulations of this work. In each panel, the short-dashed curve represents the analytic best fit of the distribution, while the long-dashed curve represents the distribution found for DM haloes by Wetzel (2011, specifically for $z = 0$ and host-halo mass $10^{13.5}\,\mathrm{M}_{\odot}$; see section 6 in that paper). In the right-hand panel, the results of Wetzel (2011) are rescaled by identifying the virial radius with r_{cen}.

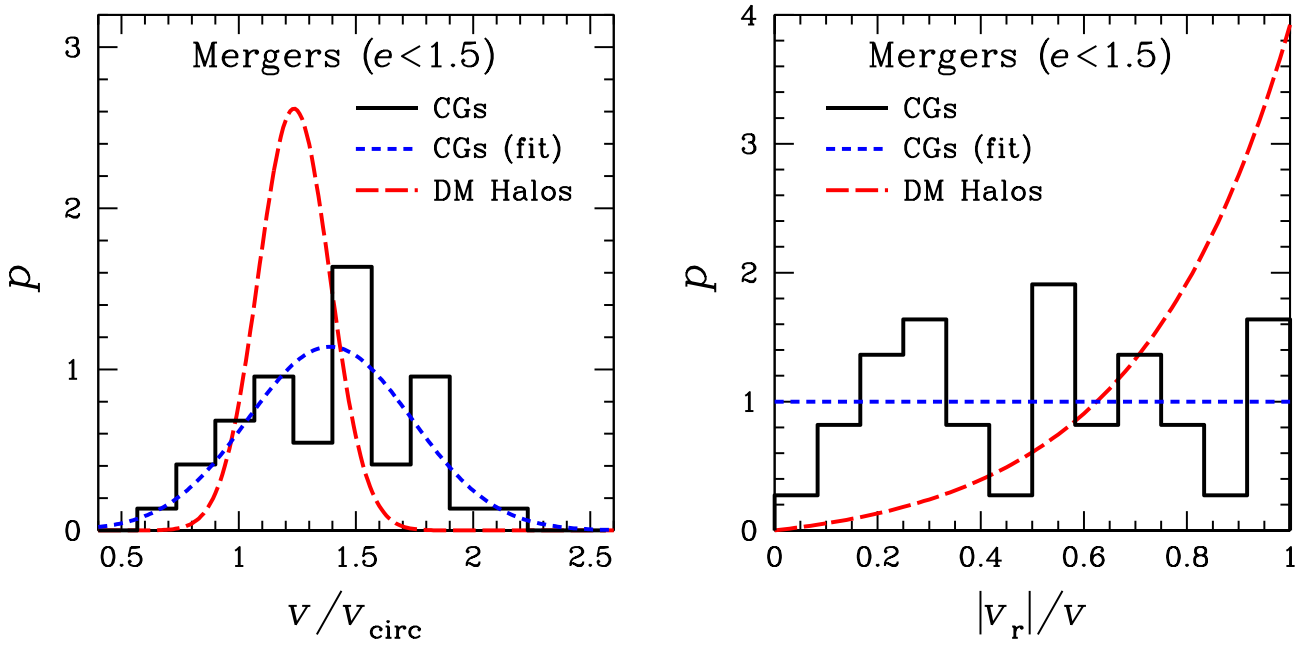

Figure 10. Probability distribution $p = \mathrm{d}n/\mathrm{d}x$ of the final speed ($x = v/v_{\mathrm{circ}}$; left-hand panel, solid histogram) and radial velocity component ($x = |v_r|/v$; right-hand panel, solid histogram) for mergers in the simulations of this work. In each panel, the short-dashed curve represents the analytic best fit of the distribution, while the long-dashed curve represents the distribution found for DM haloes by Jiang et al. (2015, specifically host-halo mass $10^{14}\,\mathrm{M}_{\odot}$ and satellite-to-host mass ratio 0.005–0.05; see section 3.4 in that paper). For the CGs studied in this paper, we take as reference radius r_{cen}, so $v_{\mathrm{circ}} = \sigma_{\mathrm{cen}}$. For the cosmological haloes of Jiang et al. (2015), v_{circ} is the circular velocity at the virial radius, at which v and v_r are measured.

Table 2. Mean (μ) and standard deviation (σ) of the distributions of the orbital parameters (η, $r_{\rm peri,\,2b}/r_{\rm cen}$, $v/v_{\rm circ}$ and $|v_r|/v$) for the central-satellite mergers of our simulations (CGs) and for accretion of cosmological satellites (DM haloes). The data for cosmological satellites are taken from Wetzel (2011) and Jiang et al. (2015), as indicated in the captions of Figs 9 and 10.

	$\mu(\eta)$	$\sigma(\eta)$	$\mu(r_{\rm peri,\,2b}/r_{\rm cen})$	$\sigma(r_{\rm peri,\,2b}/r_{\rm cen})$	$\mu(v/v_{\rm circ})$	$\sigma(v/v_{\rm circ})$	$\mu(\lvert v_r\rvert/v)$	$\sigma(\lvert v_r\rvert/v)$
CGs	0.64	0.28	0.50	0.32	1.39	0.35	0.53	0.27
DM haloes	0.51	0.22	0.24	0.22	1.24	0.15	0.79	0.19

viral radius. Moreover, the scatter in the orbital parameters tends to be larger for accretion on to CGs than for accretion on to cosmological haloes.

5 DISCUSSION

The results of this work are based on an admittedly idealized models, which rely on a few simplifying assumptions. Here we discuss these assumptions and their possible implications.

5.1 Initial distribution of satellite orbits

In our model, we have assumed that the system of satellite galaxies is initially in equilibrium in the gravitational potential of the host (Section 2). Though this is clearly an idealization, this assumption is probably the most reasonable in the framework of simple models that do not account explicitly for the cosmological framework in which the host halo evolves. As an alternative, one would be tempted to consider as initial distributions of the orbital parameters of the satellites the distributions measured for infalling DM haloes in cosmological *N*-body simulations. However, there are reasons to believe that infalling cosmological satellites at their first pericentric passage do not contribute significantly to accretion on to the CG. This can be quantitatively shown by the following argument. Let us consider, for instance, the distributions of the orbital parameters measured by Jiang et al. (2015) for cosmological infalling haloes, which is expressed in terms of $v/v_{\rm circ}$ and $|v_r|/v$ as measured at the virial radius r_{200} (see Section 4.4.3). Let us take, for example, the best-fitting distributions of $v/v_{\rm circ}$ and $|v_r|/v$ for hosts of mass $10^{14}\,{\rm M}_\odot$, and mass ratio in the range 0.005–0.05. As the distribution of $v/v_{\rm circ}$ is quite narrow, for simplicity we fix $v/v_{\rm circ} = 1.236$, the mean value of the distribution. For given $|v_r|/v$, we then integrate the orbit in the gravitational potential of an NFW halo with concentration $r_{200}/r_{\rm s} = 5$ and we look for the value of $|v_r|/v$ such that the satellite plunges down to $r = r_{\rm cen}$ in the gravitational potential of the host. It turns out that only the 0.6 per cent most radial orbits of the cosmological distribution (those with $|v_r|/v \gtrsim 0.998$) have pericentre $\lesssim r_{\rm cen}$ (see also fig. 2 in Vulcani et al. 2016a) and would be classified as an encounter. Moreover, the typical eccentricity of such encounters (in the two-body approximation) is $e \approx 10$, so virtually all of these encounters are high-speed fly-bys that do not lead to rapid mergers. In the above estimate of the fraction of cosmological orbits that reach the CG at the first pericentric passage, we have neglected dynamical friction. However, we have verified with *N*-body simulations similar to those described in Section 3 that the effect of dynamical friction, at least at the first pericentric passage, is negligible even on such very radial orbits (see also Vulcani et al. 2016a).

As the satellites are typically not accreted at their first pericentric passage, we expect that the cosmological orbital distribution is substantially modified during the global relaxation process of the host halo. Though it is not easy to predict in detail the resulting distribution, there are reasons to believe that, owing to phase mixing and violent relaxation, this distribution cannot be far from equilibrium.

5.2 Tidal stripping

In our model, we have assumed that the satellite is rigid, so the effect of tidal stripping is neglected. This simplifying assumption is justified in the considered context, because the initial time of our simulations ($t = 0$) must not be interpreted as the time of accretion of the satellite on to the host halo, but instead as a later time at which the satellite has already evolved within the halo (consistent with the assumption that the satellite's orbit is extracted from an equilibrium distribution). However, it is clear that our model is simplistic in this respect. It is well known that the combination of tidal stripping and dynamical friction leads to a complex interaction of satellite and host stellar systems, which has been studied extensively in the literature (e.g. Tormen, Diaferio & Syer 1998; Taffoni et al. 2003; Angulo et al. 2009). In particular, Boylan-Kolchin, Ma & Quataert (2008) ran simulations similar to ours, but with live satellites, therefore able to catch the combined effect of tidal stripping and dynamical friction. Boylan-Kolchin et al. (2008) quantified the effect of tidal stripping on the merging time-scale (as the satellite loses mass, the dynamical-friction time-scale gets longer), but do not study in detail the evolution of orbital parameters of rigid and live satellites. Our pairs of simulations with the same initial orbits but different satellite mass (see Fig. 3) suggest that rigid and live satellites should follow similar tracks in the orbital-parameter space, though with different rates of evolution. However, in detail, the evolution of the orbital parameters is somewhat dependent on the satellite mass (see Fig. 4).

We note that Boylan-Kolchin et al. (2008) used the results of their simulations to estimate the distribution of the circularity η of the orbits of satellites accreted by the CG, similar to what we have done in this work. Boylan-Kolchin et al. (2008) find that the distribution of η peaks at a lower value with respect to the distribution of cosmological haloes (fig. 7 in their paper), seemingly in contrast with the results of this work (Fig. 9, left-hand panel). In fact, the two results are not directly comparable, because Boylan-Kolchin et al. (2008) measure η at the time of accretion on the host halo, while we measure η at the time of the encounter with the CG. As a synthesis of the two results, we might say that, from the point of view of the host halo, only satellites that are initially on eccentric orbits are able to encounter the CG (see also Section 5.1), but, when these satellites merge with the CG, their orbits (modified by dynamical friction) tend to be preferentially tangential from the point of view of the CG.

5.3 Future of fly-bys

In our analysis, we have excluded encounters classified as fly-bys, because they are not expected to lead to rapid mergers. However, it is of course possible that at least some of such encounters will lead to mergers in a cosmologically relevant time. In principle, we could follow in our simulations the evolution of fly-bys beyond the

time ($t_{\rm fin}$) of the first encounter. However, the simulations beyond $t_{\rm fin}$ would not be very meaningful, because the rigid satellite would be a quite poor representation of a satellite passed through the host's centre, and also the host's particle distribution would be unrealistically modified by the rigid satellite orbiting through its central regions, because of dynamical-friction heating (El-Zant, Shlosman & Hoffman 2001; Nipoti et al. 2004). For these reasons, it is not easy to predict the effect on the distribution of the orbital parameters of the fly-bys that will end up merging. However, Figs 3 and 5 (in which systems with $E/E_{\rm u} \gtrsim -0.7$ are all fly-bys) suggest that at least some of these mergers might be characterized by relatively low angular momentum.

6 SUMMARY AND CONCLUSIONS

In this paper, we have studied the distribution of the orbital parameters of satellite galaxies accreted by the CGs in groups and clusters of galaxies. We have estimated the central-satellite orbital parameters with the help of somewhat idealized N-body simulations in which a massive satellite orbits in a stationary DM halo. We assume as working hypothesis that the galaxies that will end up merging with the CG originally belong to a system of satellites in equilibrium in the gravitational potential of the host. Owing to dynamical friction, the satellite loses energy and angular momentum and, in a fraction of the simulations, it encounters the CG in a cosmologically relevant time-scale. In simulations that end up with an encounter between central and satellite, we measure the orbital parameters of the encounter and we classify it either as a merger or as a fly-by. The main findings of this work are the following.

(i) We confirm and strengthen previous indications that dynamical friction does not necessarily lead to orbit circularization: The effect of dynamical friction on the orbit of the decelerated object depends not only on the host's distribution function, but also, for given distribution function, on the initial orbital parameters of the satellite.

(ii) The distributions of the orbital parameters of the central-satellite mergers are markedly different from the distributions found for halo–halo mergers in cosmological simulations.

(iii) The orbits of the satellites accreted by the CGs are, compared to those of cosmological halo–halo encounters, on average less bound, because the merger occurs at the bottom of a deep potential well, and less eccentric, because the trajectory of the satellite, shrunk by dynamical friction, is likely to end up grazing the CG.

(iv) The scatter in the orbital parameters tends to be larger for accretion on to CGs than for accretion on to cosmological haloes.

(v) We provide fits to the distributions of the central-satellite merging orbital parameters that can be used to study the merger-driven evolution of the scaling relations of CGs.

ACKNOWLEDGEMENTS

I would like to thank the referee, Jaime Perea, for the positive and constructive report, and Benedetta Vulcani for helpful comments on a draft of this paper.

REFERENCES

Angulo R. E., Lacey C. G., Baugh C. M., Frenk C. S., 2009, MNRAS, 399, 983
Arena S. E., Bertin G., 2007, A&A, 463, 921
Ascasibar Y., Gottlöber S., 2008, MNRAS, 386, 2022
Bellstedt S. et al., 2016, MNRAS, 460, 2862
Benson A. J., 2005, MNRAS, 358, 551
Bernardi M., Hyde J. B., Sheth R. K., Miller C. J., Nichol R. C., 2007, AJ, 133, 1741
Bernardi M., Roche N., Shankar F., Sheth R. K., 2011, MNRAS, 412, L6
Binney J., Tremaine S., 1987, Galactic Dynamics. Princeton Univ. Press, Princeton, NJ
Bontekoe T. R., van Albada T. S., 1987, MNRAS, 224, 349
Boylan-Kolchin M., Ma C.-P., Quataert E., 2005, MNRAS, 362, 184
Boylan-Kolchin M., Ma C.-P., Quataert E., 2006, MNRAS, 369, 1081
Boylan-Kolchin M., Ma C.-P., Quataert E., 2008, MNRAS, 383, 93
Buchan S., Shankar F., 2016, MNRAS, 462, 2001
Casertano S., Phinney E. S., Villumsen J. V., 1987, in de Zeeuw P. T., ed., Proc. IAU Symp. 127, Structure and Dynamics of Elliptical Galaxies. Reidel, Dordrecht, p. 475
Chandrasekhar S., 1943, ApJ, 97, 255
De Lucia G., Blaizot J., 2007, MNRAS, 375, 2
Diemand J., Moore B., Stadel J., 2004, MNRAS, 352, 535
Dubinski J., 1998, ApJ, 502, 141
El-Zant A., Shlosman I., Hoffman Y., 2001, ApJ, 560, 636
Feldmann R., Carollo C. M., Mayer L., Renzini A., Lake G., Quinn T., Stinson G. S., Yepes G., 2010, ApJ, 709, 218
Gill S. P. D., Knebe A., Gibson B. K., Dopita M. A., 2004, MNRAS, 351, 410
Gnedin O. Y., Ostriker J. P., 1997, ApJ, 474, 223
Gnedin O. Y., Ostriker J. P., Tremaine S., 2014, ApJ, 785, 71
Hashimoto Y., Funato Y., Makino J., 2003, ApJ, 582, 196
Hausman M. A., Ostriker J. P., 1978, ApJ, 224, 320
Iannuzzi F., Dolag K., 2012, MNRAS, 427, 1024
Jiang L., Cole S., Sawala T., Frenk C. S., 2015, MNRAS, 448, 1674
Khochfar S., Burkert A., 2006, A&A, 445, 403
Lindblad B., 1933, Handbuch der Astrophysik, Vol. 5. Springer-Verlag, New York, p. 937
Liu F. S., Xia X. Y., Mao S., Wu H., Deng Z. G., 2008, MNRAS, 385, 23
Londrillo P., Nipoti C., Ciotti L., 2003, Mem. Soc. Astron. Ital., 1, 18
Lynden-Bell D., 1967, MNRAS, 136, 101
Marchesini D. et al., 2014, ApJ, 794, 65
Merritt D., 1985, ApJ, 289, 18
Montero-Dorta A. D., Shu Y., Bolton A. S., Brownstein J. R., Weiner B. J., 2016, MNRAS, 456, 3265
Naab T., Johansson P. H., Ostriker J. P., 2009, ApJ, 699, L178
Navarro J. F., Frenk C. S., White S. D. M., 1996, ApJ, 462, 563 (NFW)
Nipoti C., Londrillo P., Ciotti L., 2003a, MNRAS, 342, 501
Nipoti C., Stiavelli M., Ciotti L., Treu T., Rosati P., 2003b, MNRAS, 344, 748
Nipoti C., Treu T., Ciotti L., Stiavelli M., 2004, MNRAS, 355, 1119
Nipoti C., Treu T., Bolton A. S., 2009, ApJ, 703, 1531
Nipoti C., Treu T., Leauthaud A., Bundy K., Newman A. B., Auger M. W., 2012, MNRAS, 422, 1714
Osipkov L. P., 1979, Sov. Astron. Lett., 5, 42
Ostriker J. P., Tremaine S. D., 1975, ApJ, 202, L113
Perea J. D., Solanes J. M., 2016, MNRAS, 461, 344
Posti L., Nipoti C., Stiavelli M., Ciotti L., 2014, MNRAS, 440, 610
Ruszkowski M., Springel V., 2009, ApJ, 696, 1094
Shankar F. et al., 2015, ApJ, 802, 73
Solanes J. M., Perea J. D., Darriba L., García-Gómez C., Bosma A., Athanassoula E., 2016, MNRAS, 461, 321
Statler T. S., 1991, ApJ, 375, 544
Taffoni G., Mayer L., Colpi M., Governato F., 2003, MNRAS, 341, 434
Taranu D. S., Dubinski J., Yee H. K. C., 2013, ApJ, 778, 61
Taranu D., Dubinski J., Yee H. K. C., 2015, ApJ, 803, 78
Tonini C., Bernyk M., Croton D., Maraston C., Thomas D., 2012, ApJ, 759, 43
Tormen G., Diaferio A., Syer D., 1998, MNRAS, 299, 728
Tremaine S., 1990, in Wielen R., ed., Dynamics and Interactions of Galaxies. Springer-Verlag, Berlin, Heidelberg, p. 394
Tremaine S. D., Ostriker J. P., Spitzer L., Jr, 1975, ApJ, 196, 407
Tsuchiya T., Shimada M., 2000, ApJ, 532, 294
van den Bosch F. C., Jiang F., 2016, MNRAS, 458, 2870
van den Bosch F. C., Lewis G. F., Lake G., Stadel J., 1999, ApJ, 515, 50

Vulcani B. et al., 2014, ApJ, 797, 62
Vulcani B. et al., 2016a, ApJ, preprint (arXiv:1610.04615)
Vulcani B. et al., 2016b, ApJ, 816, 86
Wetzel A. R., 2011, MNRAS, 412, 49
White S. D. M., 1976, MNRAS, 174, 19
Wojtak R., Gottlöber S., Klypin A., 2013, MNRAS, 434, 1576

APPENDIX A: FINAL DISTRIBUTIONS OF THE ORBITAL PARAMETERS FOR ISOTROPIC AND ANISOTROPIC FAMILIES OF MODELS

In this appendix, we compare the distributions of the final orbital parameters of central-satellite encounters in families of models with isotropic (I1, I5) and anisotropic (A1, A5) distribution functions. Fig. A1 plots the cumulative distributions of specific energy E_{2b} (in the two-body approximation; left-hand panel) and angular-momentum modulus L (right-hand panel) for the isotropic and anisotropic cases. According to a Kolmogorov–Smirnov test, the probabilities that the final distributions of E_{2b} and L in the isotropic and anisotropic cases are extracted from the same parent distributions are 0.09 for E_{2b} and 0.63 for L. Therefore, the differences between the isotropic and anisotropic cases are more significant in the distribution of E_{2b} than in the distribution of L, but also for E_{2b} the result of the Kolmogorov–Smirnov test does not provide compelling evidence that the final distribution of orbital energies is different in the two families of models.

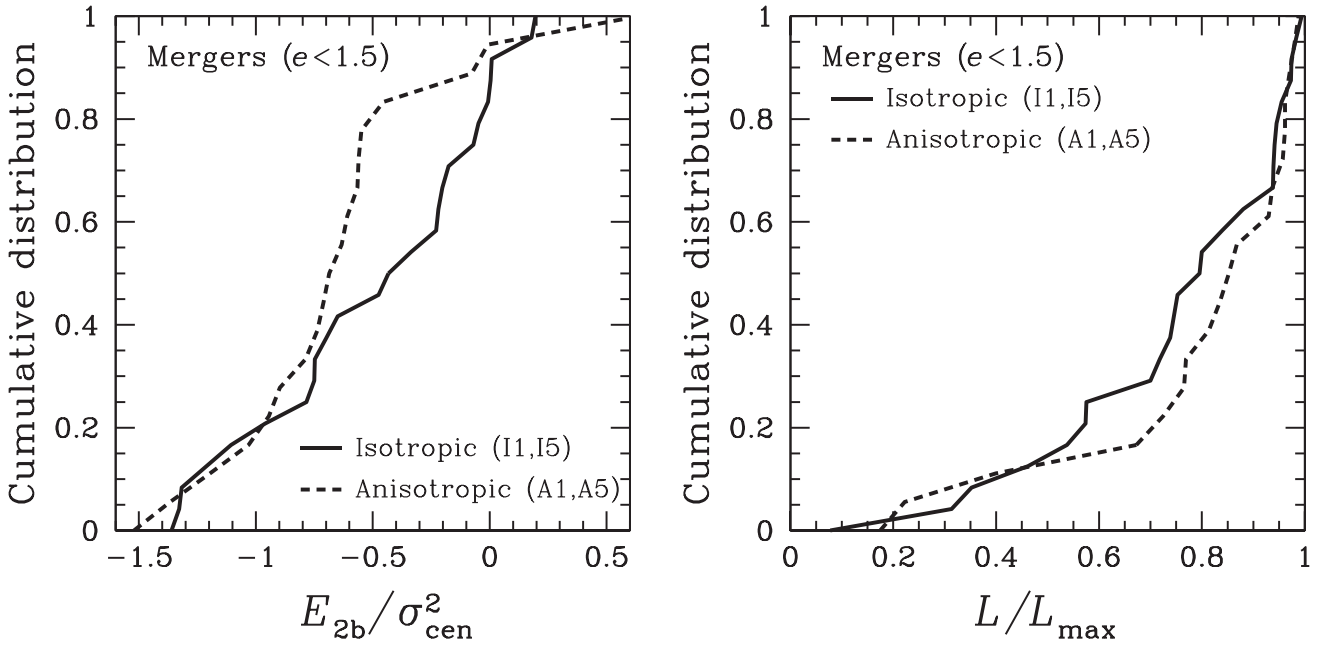

Figure A1. Cumulative distribution of the final specific orbital energy, computed in the two-body approximation (E_{2b}/σ^2_{cen}; left-hand panel, solid histogram), and angular-momentum modulus (L/L_{max}; right-hand panel, solid histogram) for isotropic (solid line) and anisotropic (dashed line) families of models. σ_{cen} is the characteristic velocity dispersion of the CG and L_{max} is defined by equation (8).

This paper has been typeset from a TEX/LATEX file prepared by the author.